Ann. Rev. Nucl. Part. Sci. 1986. 36 : 683–716

NUCLEAR SHAPES STUDIED BY COULOMB EXCITATION

Douglas Cline

Nuclear Structure Research Laboratory,[1] University of Rochester, Rochester, New York 14627

CONTENTS

1. INTRODUCTION AND OVERVIEW

Nuclear excitation caused by the time-dependent electromagnetic field acting between colliding atomic nuclei is called Coulomb excitation. For bombarding energies well below the Coulomb barrier, the colliding nuclei remain sufficiently far apart to ensure that the finite-range nuclear interaction is insignificant and thus the interaction is dominated by the well-known electromagnetic force. The importance of Coulomb excitation lies in the fact that the theory is well understood, allowing for quantitative

[1] Supported by the National Science Foundation.

0163–8998/86/1201–0683$02.00

studies of nuclear structure unimpeded by uncertainties in our knowledge of the interaction and reaction mechanism that plague many other spectroscopic probes employed in nuclear science.

Collective quadrupole rotational and vibrational modes of motion are a dominant and ubiquitous feature of low-lying spectra in nuclei. For strongly deformed nuclei the excitation energies of the ground-state rotational band exhibit a rotational behavior, i.e. $E_I = I(I+1)\hbar^2/2\mathcal{I}$, where I is the spin and $\mathcal{I}$ the moment of inertia is approximately a third of the rigid rotor value at low spin and increases smoothly with increase in spin. Moreover, the E2 transition strengths for these ground-state rotational bands are enhanced up to ~ 300 single-particle units, which is consistent with collective rotation of the nucleus. The Bohr & Mottelson model (1, 2) ascribes the quadrupole collectivity to collective rotations and vibrations of a quadrupole-shaped nucleus. In this picture the instantaneous quadrupole shape, at a time t, of a density contour ρ can be defined in any frame of reference as

$$R(\theta, \phi, t, \rho) = R_0(\rho)\left[1 + \sum_{\mu} (-)^{\mu} \alpha^2_{-\mu}(t, \rho) Y_{2,\mu}(\theta, \phi)\right].$$

The understanding of such shapes is facilitated by making a transformation into the instantaneous principal axis frame specified by two nonzero parameters α^2_0 and α^2_2 and the three Euler angles defining the principal axis frame. It is usual to express the two body-fixed quadrupole deformation parameters in terms of Bohr's parameters, β, γ, defined by $\alpha^2_{+2} = \alpha^2_{-2} = (\beta/\sqrt{2})\sin\gamma$, $\alpha^2_{+1} = \alpha^2_{-1} = 0$, and $\alpha^2_0 = \beta\cos\gamma$. The parameter β specifies the magnitude of the quadrupole deformation, while γ specifies the asymmetry of the shape, i.e. $\gamma = 0°$ is prolate, $\gamma = 60°$ is oblate, and $0 < \gamma < 60°$ corresponds to triaxial deformed shapes.

The E2 properties of the states are the most direct and unambiguous measure of the collective shape parameters for quadrupole collective modes. Coulomb excitation selectively excites low-lying collective bands with cross sections that are the direct measure of the Eλ matrix elements involved in the excitation. Mottelson (3) was the first to recognize that E2 Coulomb excitation is the preeminent probe for studying quadrupole collective motion in nuclei. Coulomb excitation was first observed in 1953 (4, 5) and the early work played a pivotal role in the development of the Bohr & Mottelson (1, 2) collective model. The theoretical foundation of Coulomb excitation was summarized in the 1956 landmark review paper by the Copenhagen group (6) although the origin of the theory can be traced back to the 1913 paper of Bohr (7) on atomic Coulomb excitation. The early history and theory of Coulomb excitation are discussed in three

books (8–10) while several review articles outline the progress in this field (6, 11–18).

The early Coulomb excitation experiments employed light ions for which only single-step Coulomb excitation is important and the electromagnetic interaction is sufficiently weak to allow analysis using simple first-order theory (6). When high-Z projectiles are used, the electromagnetic interaction becomes sufficiently strong to make multistep excitation of the target probable, and this leads to the population of many more excited states. Such multiple Coulomb excitation was observed first in 1958 (19, 20). Coulomb excitation received a new vitality in the 1960s with the commissioning of new heavy-ion accelerators and the development of the Ge(Li) high-resolution gamma-ray detector used for observing the deexcitation of the collective bands excited by multiple Coulomb excitation. However, the crucial advance was the development of the semiclassical coupled-channel Coulomb excitation computer code of Winther & de Boer (21), which was essential for analyzing the data from these more complicated experiments.

A renaissance in the field of Coulomb excitation has resulted from the ability of the latest generation of heavy-ion accelerators to provide copious beams of all stable nuclei with energies up to 5 MeV per nucleon; especially the highest Z beams, such as ^{208}Pb. Now it is feasible, using high-Z projectiles, to Coulomb excite the lowest state of each spin, the yrast sequence, to spin $30\hbar$ in strongly deformed actinide nuclei and to excite lower-spin collective states lying within 2 MeV of the yrast sequence. The availability of such heavy-ion beams stimulated the development of new high-efficiency detector systems able to resolve the complicated gamma-ray deexcitation of the many states Coulomb excited when high-Z projectiles are employed.

The latest advance in the field of Coulomb excitation has been the development of Coulomb excitation least-squares search codes (22, 23) capable of extracting from heavy-ion-induced Coulomb excitation data almost the complete set of ~ 100 E2 matrix elements coupling the many (~ 30) states involved in the excitation process. Thus, after thirty years of work in this field, it is possible finally to exploit the powerful technique of Coulomb excitation to measure essentially all the E2 matrix elements for low-lying nuclear levels. The completeness and extent of this E2 information is sufficient to determine the centroids and fluctuation widths of the quadrupole deformation for several low-lying states; this adds a new dimension to the study of quadrupole collectivity in nuclei. In particular, the completeness of the E2 data makes it practical to exploit a model-independent sum-rule method (24–26) to project the intrinsic frame E2 properties directly from this large body of data. These properties are

important because they determine the quadrupole collective shape parameters and provide considerable insight into the role of collective motion in nuclei.

This review outlines the recent advances in the field of heavy-ion multiple Coulomb excitation and focuses on those aspects that make it feasible to measure essentially all the E2 matrix elements for low-lying states in stable nuclei. The scope, accuracy, and limitations of this new capability are summarized here. Coulomb excitation is a highly selective probe of collective shape degrees of freedom, and examples are presented to illustrate how this feature is used to study quadrupole collectivity in both strongly deformed and shape transitional nuclei. The interpretation in terms of fluctuating shape degrees of freedom of the large data sets, resulting from multiple Coulomb excitation, is a second aspect reviewed.

The recent developments provide a powerful spectroscopic probe of nuclear shapes. These are being used to answer important open questions in nuclear structure such as (*a*) the limits of validity of macroscopic collective models, (*b*) the role of symmetries in collective motion, (*c*) the existence of shape transitions and shape coexistence, and (*d*) the interplay of single-particle and collective degrees of freedom in nuclear structure. An overview is presented of the nuclear structure implications of the recent Coulomb excitation work and the outlook for applying this technique to probe unexplored areas of nuclear structure.

2. THEORY OF COULOMB EXCITATION

A comprehensive presentation of the theory of Coulomb excitation is beyond the scope of this review. The purpose of this chapter is to mention only those features of the theory necessary to an understanding of the methods and results presented in this review. For more details of the theory the reader is referred to the excellent and thorough presentation in the book by Alder & Winther (10).

The basic assumption of Coulomb excitation is that the interaction is purely electromagnetic. It is crucial to know the maximum bombarding energy consistent with the above basic assumption since multiple excitation of the highest spin members of collective bands requires the highest bombarding energy. Experimental data on the Coulomb-nuclear interference effect have been used to estimate the maximum bombarding energy at which the influence of nuclear excitation can be neglected, i.e. $<0.1\%$, leading to a conservative crude safe bombarding-energy criterion (14, 27–30) that the distance of closest approach for a head-on collision must exceed $[1.25(A_P^{1/3}+A_T^{1/3})+5]$ fm. This corresponds to bombarding energies below 4.5 MeV per nucleon for ^{208}Pb projectiles decreasing to less than 4.1

MeV per nucleon for ^{40}Ar ions. Heavy-ion Coulomb excitation experiments have been performed at up to 5.3 MeV per nucleon in order to maximize population of the highest spin states. Coulomb-nuclear interference effects can be minimized at energies above the Coulomb barrier by staying forward of the grazing angle, that is, by using classical trajectories where the distance of closest approach exceeds the safe distance given above.

In principle it is straightforward to evaluate the Coulomb excitation cross section if all the electric and magnetic multipole matrix elements are known for both target and projectile. Unfortunately, exact quantal coupled-channel calculations are impractical because of the long range of the Coulomb force, the small wavelength, the thousands of partial waves that contribute, and the many strongly coupled states involved in heavy-ion Coulomb excitation. Iterative techniques have been used to perform quantal coupled-channel Coulomb-excitation calculations (31, 32) for cases with a limited number of excited states. Development of an efficient quantal coupled-channel computer code capable of handling ~ 50 high-spin states is the most important task remaining for the theory of Coulomb excitation.

The semiclassical theory of Coulomb excitation assumes that nuclear excitation is caused by the time-dependent electromagnetic field acting on the colliding nuclei as the projectile moves along a classical hyperbolic trajectory in the Coulomb field of the target nucleus. The semiclassical approximation (33) provides an excellent description of the scattering process for heavy-ion-induced Coulomb excitation since the projectile wavelength is between 100 and 1000 times smaller than the distance of closest approach and the ratio of energy transfer to total kinetic energy is small and thus has a negligible influence on the trajectory. In the semiclassical approximation the Coulomb excitation process is described by the time-dependent Schrödinger equation (11):

$$i\hbar\dot{\psi}(t) = [H_0 + V(t)]\psi(t),$$

where H_0 is the intrinsic free Hamiltonian and $V(t)$ is the time-dependent electromagnetic interaction as the scattering nuclei follow the classical equations of motion. Expanding the wave function in terms of the eigenstates of the unperturbed nuclei, i.e.

$$\psi(t) = \sum_n a_n(t)\phi_n,$$

produces a set of coupled differential equations for the time-dependent excitation amplitudes $a_n(t)$,

$$i\hbar\dot{a}_n(t) = \Sigma_m \langle n|V(t)|m\rangle \exp[i(E_n - E_m)t/\hbar]a_m(t).$$

These equations are solved with the condition that the two nuclei initially are in their ground states. The electromagnetic interaction, $V(t)$, between the two extended nuclei can be expanded in terms of electric and magnetic multipoles. The kinetic energy of the centers of mass of the two colliding nuclei as well as the monopole-monopole interaction are incorporated implicitly in determining the classical trajectory. In Coulomb excitation experiments it is normal to choose one of the colliding nuclei to have a ground-state spin of zero and a high-lying first excited state to ensure that only one of the colliding nuclei is excited significantly. Thus only the monopole-multipole interaction is significant, which simplifies the calculations as well as resulting in simpler experimental spectra. Moreover, the magnetic interaction is small in heavy-ion Coulomb excitation because the safe bombarding-energy criterion requires that $(v/c)^2 < 0.01$. The semiclassical coupled-channel computer code of Winther & de Boer (21) computes the differential cross sections for a given set of initial conditions and electromagnetic matrix elements. This code has played a key role in the field of Coulomb excitation for two decades.

The semiclassical coupled-channel calculations need to be corrected for several small systematic errors, the first of which is due to the deficiency of the semiclassical approximation. The use of symmetrized orbits in semiclassical calculations approximately corrects for transfer of energy to excitation of the nuclei, which is one source of error. The quantal calculations of Tolsma (31) for excitation of the ground band of ^{238}U by 385-MeV ^{84}Kr ions show that the semiclassical cross sections differ from the quantal predictions by 0 to 10% depending on the spin of the state and the scattering angle. However, analysis of heavy-ion-induced Coulomb excitation data usually involves a comparison of the deexcitation gamma-ray yields of the excited states, which tends to cancel part of this error. For example, Stachel et al (34) compared semiclassical with quantal calculations for Coulomb excitation of ^{104}Ru by 4.6-MeV per nucleon ^{208}Pb ions and they found that the ratio of the gamma-ray yields deexciting adjacent states predicted by the two calculations differ by 1 to 3%. The classical Rutherford orbit is perturbed slightly by atomic screening, vacuum polarization, relativistic effects, and electric dipole polarization of the nuclei. These effects change slightly the distance of closest approach and can be taken into account by making a small net change of $\sim$0.3% in the bombarding energy (10). Virtual excitation of the giant dipole resonance also contributes to nuclear excitation because classically the dipole polarization differs for the three axes of a deformed nucleus, contributing a dipole torque in addition to the quadrupole torque. This effect decreases the predicted gamma-ray yields of high-spin states by only $\sim$4–12% and

is estimated adequately by adding a polarization term to the interaction (10).

The deexcitation gamma-ray angular distributions can be appreciably perturbed by the deorientation effect, i.e. the hyperfine interaction of the excited nuclear states with the several megagauss magnetic fields produced by the highly ionized atomic shell of the excited nucleus recoiling in vacuum. The deorientation effect constitutes the most important correction to the analysis of most Coulomb excitation experiments. Neither the magnetic moments of the excited states nor the hyperfine magnetic fields caused by the excited atomic shell are known, nor are the contributions of electric hyperfine interactions, so models must be used with parameters fitted to measured gamma-ray angular distributions. The Abragam & Pound (35) model of an isotropic, randomly fluctuating magnetic field caused by deexcitation of the highly excited atomic shell has been used in the analysis of some experiments (34). The Rochester collaboration (18) uses the two-state model of Brenn et al (36), which extends the Abragam & Pound model by adding a quasi-static field compared to the lifetimes of the nuclear states. Although the deorientation effect appreciably perturbs the angular correlation of the deexcitation gamma rays, the overall effect is small in most experiments and the error introduced is less than that due to statistical uncertainties. For example, the adopted uncertainty in the deorientation effect changed the transition E2 matrix elements by at most 2% for ^{186,188,190,192}Os and ^{194}Pt (37, 38).

In summary, the semiclassical Coulomb excitation computer codes are currently the only viable means of analyzing heavy-ion Coulomb excitation data. The dimension of the problem exceeds the capability of available quantal computer codes. The error introduced by the semiclassical approximation plus the other small correction terms lead to a total uncertainty of $\sim 5\%$ in the predicted cross sections and yields, which is comparable to the statistical uncertainties in most experiments.

3. EXPERIMENTAL TECHNIQUES

The double closed-shell nucleus ^{208}Pb is ideal for Coulomb excitation studies because of its high charge ($Z = 82$) and because excitation of the first excited 3^- state at 2.6 MeV is negligible. Much of the recent heavy-ion Coulomb excitation work has centered around target excitation using 4.5 MeV per nucleon beams of ^{208}Pb and single closed-shell nuclei such as ^{136}Xe and ^{142}Nd from two major heavy-ion linear accelerators, namely, the SuperHILAC at the Lawrence Berkeley Laboratory and the UNILAC at the Gesellschaft für Schwerionenforschung (GSI) in Darmstadt. Valuable

complementary studies have been performed using ^{58}Ni, ^{40}Ca, ^{32}S, and ^{16}O beams from the larger tandem Van de Graaff accelerators such as the MP tandem at Rochester. In addition, projectile excitation by ^{208}Pb targets also has proved to be a valuable technique and some such studies have been performed using tandem Van de Graaff accelerators (39).

Gamma-ray spectroscopy using Ge gamma detectors is the only viable experimental technique for resolving the many states Coulomb excited when heavy ions are utilized. Unfortunately, the recoil velocities of the excited target nuclei can be large, $v/c = 0.1$, which leads to considerable Doppler shift and Doppler broadening of detected gamma rays. Use of a target thick enough to stop the recoiling excited nuclei produces Doppler-broadened gamma-ray line shapes because the lifetimes of high-spin states are comparable to the slowing down time of the recoiling ion in the target. The problem of Doppler broadening can be overcome by using thin targets so that the excited nuclei recoil into vacuum, and also by observing the deexcitation γ rays in coincidence with scattered ions detected at known scattering angles, in order to specify the recoil direction and velocity. Thus the individual γ-ray signals can be corrected for the Doppler shift on an event-by-event basis. The optimum γ-ray energy resolution is achieved by minimizing the solid angle of the Ge detector and by placing it in the recoil direction where the Doppler shift is a maximum and the Doppler broadening, due to the finite size of the Ge detector, is minimized.

Most of the heavy-ion-induced Coulomb excitation experiments have employed variants of the experimental geometry (40, 41) illustrated in Figure 1. Such experimental geometries provide Coulomb excitation data simultaneously over a wide range of scattering angles, or equivalently, Coulomb excitation strength, which is crucial for analyzing the data as discussed later. Figure 2 illustrates a typical Doppler-corrected γ-ray spectrum obtained with such an arrangement (42). The high selectivity of Coulomb excitation is reflected by the simplicity of such spectra.

The optimum geometry for the particle detectors depends on the mass ratio of the projectile and target. For heavy projectiles, such as ^{208}Pb, on lighter-mass target nuclei, i.e. when $M_P > M_T$, the scattered projectiles are kinematically focussed forward within a maximum angle θ_{max} where $\sin\theta_{max} = M_T/M_P$. Annular detectors at forward angles can be used to detect, with nearly 100% efficiency, all of the range of scattering angles of interest. A disadvantage is that this approach leads to large recoil velocities and concomitant Doppler broadening. The alternative of projectile excitation of the lighter mass on a heavy-mass target leads to low energies of the backscattered projectiles and this can cause technical difficulties, but the lower recoil velocity produces less Doppler broadening.

The high selectivity of Coulomb excitation has allowed the decay scheme

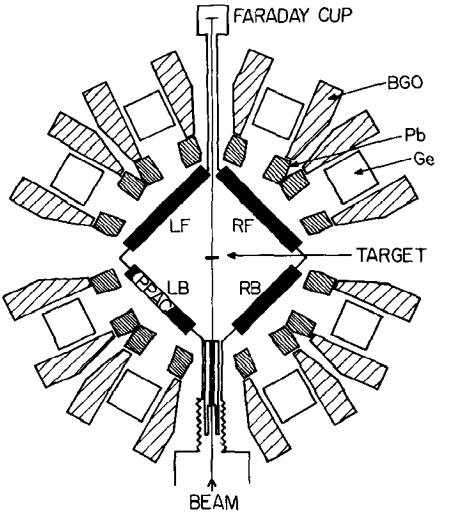

Figure 1 Schematic view of the apparatus used for heavy-ion Coulomb excitation experiments by the Rochester group (40, 41). A large solid-angle (3.9 sr) position-sensitive, parallel-plate, avalanche detector array detects both the scattered projectile and ejectile in kinematic coincidence, as well as in coincidence with an array of Compton-suppressed Ge detectors observing the deexcitation γ rays. The particle detectors measure both θ and ϕ in the range $8° < \theta < 76°$, $104° < \theta < 164°$, and $-35° < \phi < 35°$. The 0.8° angle resolution and 0.6 ns time resolution of the particle detectors are sufficient to resolve the various kinematic solutions by both the correlation of the scattering angles and the time-of-flight difference.

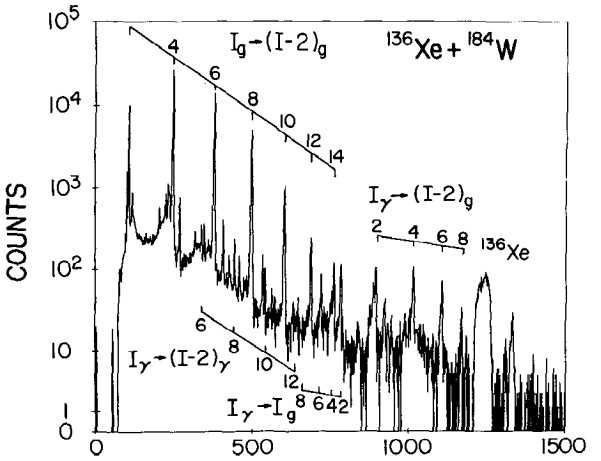

Figure 2 Coincident γ-ray spectrum for Coulomb excitation (42) of ^{184}W by 4.125 MeV per nucleon ^{136}Xe detected at scattering angles between 54° and 74° using the experimental geometry shown in Figure 1. The spectrum has been corrected for the Doppler effect on an event-by-event basis resulting in a γ-ray energy resolution of 0.5% FWHM.

and spin values of the excited states to be deduced unambiguously from (*a*) the magnitude of the γ-ray yields, (*b*) the scattering angle dependence, (*c*) the excitation functions, (*d*) projectile Z dependence, (*e*) measurements of the γ-ray multiplicity, and (*f*) the γ-ray angular distributions. Arrays of Ge detectors now coming into operation make it possible to perform useful γ-γ coincidence experiments providing valuable additional information. Moreover, such arrays allow use of smaller solid angles for individual Ge detectors, which reduces the Doppler broadening effect.

4. EXTRACTION OF ELECTROMAGNETIC MATRIX ELEMENTS FROM COULOMB EXCITATION DATA

The analysis of multiple Coulomb excitation data is difficult because of the dramatic increase in the number of matrix elements involved when many states are excited. The cross sections depend in a complicated nonlinear way on both the signs and magnitudes of many Eλ matrix elements, while M1 matrix elements are needed to account for the deexcitation gamma decay. For example, Coulomb excitation of ^{165}Ho by ^{208}Pb (43) requires calculations involving $\sim$40 levels coupled by $\sim$200 matrix elements. The problem of extracting electromagnetic matrix elements from multiple Coulomb excitation data in a model-independent way delayed exploitation of this technique for several years. The relevant questions are (*a*) can sufficient data be obtained to overdetermine the many unknown matrix elements? and (*b*) how practical is it to make a 200-dimensional search of about a thousand data when so many strongly coupled channels are needed in the calculations?

Initially, heavy-ion Coulomb excitation data were analyzed by comparing the data with semiclassical calculations employing matrix elements derived from various collective models. Conclusions drawn from such model-dependent comparisons are unreliable, as illustrated by the fact that the measured Coulomb excitation of ^{192,194,196}Pt by ^{136}Xe was well reproduced by the predictions of an incorrect model (44). Subsequent model-independent analyses (37, 38) of these data showed that this agreement was fortuitous.

Figure 3 shows the excitation probabilities for Coulomb exciting the ground-state rotational band of ^{246}Cm by backscattered projectiles. The excitation probabilities in the plateau region depend in a complicated nonlinear way on many E2 matrix elements, whereas the ratio of the probabilities for adjacent states lying in the exponential fall-off region depends most sensitively on the B(E2) connecting these states. The location of the high-sensitivity fall-off region can be moved to other spin values by

varying the scattering angle, the projectile Z, or the bombarding energy as illustrated in Figure 3. The GSI collaboration (17) studies the angular distribution over a wide range of scattering angles for a single projectile, uusually ^{208}Pb, since such data can be obtained simultaneously with the detector systems employed. The Rochester-based collaboration (18) uses both the angular distribution and the Z dependence to provide a more extensive and sensitive data set. Although this requires performing additional experiments with the lighter ions, such as ^{16}O, ^{32}S, ^{40}Ca, ^{58}Ni, the advantages of using lighter ions are (*a*) lower recoil velocities lead to smaller Doppler broadening; (*b*) cleaner γ-ray spectra allow measurements of excitation probability more than an order of magnitude lower than with heavier ions, thus the high-sensitivity region covers a wider range of states and virtual excitation of unobserved states is less of a problem in the analysis of lighter-ion data; (*c*) population of the ground band is less dominant, with lighter ions making them more suited to studies of side bands; and (*d*) the reduction in the number of states excited leads to fewer ambiguities in analysis of the data.

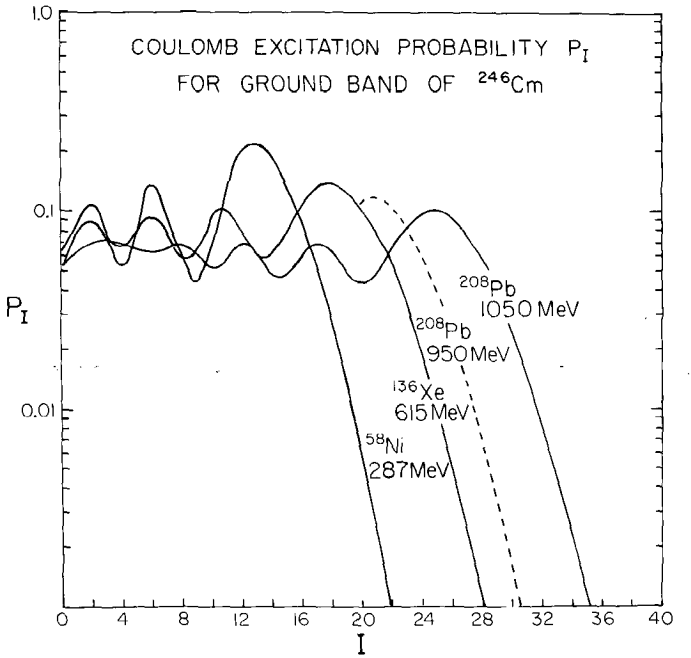

Figure 3 The calculated probability for Coulomb excitation of the ground band of ^{246}Cm by backscattered ions. The E2 matrix elements were assumed to be related by the spheroidal rotor relation.

The ratio of yields of gamma rays deexciting adjacent states of a rotational band, i.e. $R^I = Y(I+2 \rightarrow I)/Y(I \rightarrow I-2)$ is especially sensitive to the $B(\mathrm{E2}; I \rightarrow I+2)$ for states in the exponential fall-off region. Early heavy-ion Coulomb excitation work (45–47) utilized this analysis method to extract $B(\mathrm{E2})$ values for ground-state rotational bands. Model-dependent assumptions were made to account for the important influence of static electric quadrupole moments and side bands but these assumptions are reasonably valid for the strongly deformed nuclei studied. The GSI collaboration has analyzed much of their data by employing a refined version of this technique (17) in which they calculate a sensitivity matrix $S_I(\theta, J', J)$ defined by

$$\frac{\Delta R(\theta, I)}{R(\theta, I)} = S_I(\theta, J', J) \frac{\Delta \langle J' \| \mathrm{E2} \| J \rangle}{\langle J' \| \mathrm{E2} \| J \rangle},$$

which measures the change in $R(\theta, I)$ related to the variations of the matrix element $\langle J' \| M(\mathrm{E2}) \| J \rangle$. Some of the information content of the data can be ignored by this procedure and it is not suited to analysis of shape transitional nuclei where each state may be strongly coupled to many other states.

An exhaustive and exhausting investigation (48) demonstrated that Coulomb excitation data recorded using a wide range of scattering angles and projectile Z values, namely ^{16}O, ^{58}Ni, and ^{208}Pb, are sufficient to determine unambiguously the magnitudes and relative signs of 89 E2 matrix elements, both diagonal and off-diagonal, for the several low-lying collective bands of the shape transitional nucleus ^{110}Pd. The enormity of this task plus the difficulty of proving the uniqueness of the result stimulated the development in 1980 of the Coulomb excitation least-squares search code GOSIA (22).

A least-squares search can require up to 10^5 calculations of a 50-level coupled-channel system in order to locate the minimum χ^2. The Winther & de Boer (21) semiclassical Coulomb excitation code was designed to compute the cross sections for given input conditions, which is the inverse of that required by a search procedure. Moreover, this code does not calculate the γ-ray deexcitation and is orders of magnitude too slow for use in a least-squares search procedure. GOSIA (22) solves this difficult problem by using fast, analytical approximations to increase by several orders of magnitude the speed for calculation of the derivatives needed for the steepest-descent minimization. This code can make a least-squares fit of $\leqq 200$ matrix elements of various multipolarities to several thousand data from up to 50 independent Coulomb excitation experiments as well as other lifetime, branching ratio, and E2/M1 mixing ratio data. The code allows integration over solid angles of the detectors and energy loss in the

target. The deorientation effect and recoil motion are included in calculating the angular distribution of deexcitation gamma rays. Model independence is achieved by using a set of random numbers as initial values for the unknown matrix elements in the least-squares search to eliminate any bias. The uniqueness of the final solution is tested by repeating the least-squares search using various sets of random numbers as starting values for the unknown matrix elements.

The errors of the fitted matrix elements are difficult to estimate because of the dominance of the cross-correlation effects for this strongly coupled nonlinear system. Several techniques have been used to estimate the errors. In principle, sampling the χ^2 distribution along the axes indicated by the eigenvectors of the curvature matrix is an efficient means of locating the cross-correlation axes. Unfortunately, the parabolic approximation, assumed by the curvature matrix approach, is invalid for this nonlinear problem. Moreover, the usual procedure of defining an error contour (49) based on the number of degrees of freedom is problematic because both the number of data and the number of unknowns are ill defined. The approach employed is to construct the probability distribution in the space of the fitted parameters and to request the total integrated probability to be equal to the confidence limit chosen, i.e. 68.3%.

Recently Grein et al (23) developed a search code for analyzing multiple Coulomb excitation data. They assume a linear expansion of the calculated γ yields Y_i with respect to the Eλ matrix elements $\{M_j\}$:

$$Y_i(\{M_j+\Delta M_j\}) = Y_i(\{M_j\}) + \sum_j C_i(M_j,\theta)\cdot\Delta M_j.$$

The expansion coefficients $C_i(M_j,\theta)$ are evaluated numerically. Essentially they are the elements of the $S_I(\theta,J',J)$ matrix defined earlier. Some parameters have a very small sensitivity to the data, which causes problems that are overcome in this program by adding nonstatistical weights to suppress the effects of the low-sensitivity terms. The minimum is located by iteration, while the errors are calculated using the full curvature matrix. There are problems associated with this approach: computation of the sensitivity matrix is time consuming; nonstatistical weights are necessary and thus this procedure is not equivalent to a full χ^2 minimization; and the curvature matrix often has nonphysical values because the parabolic approximation is not valid and the errors are symmetric, in contrast to the asymmetric experimental errors. The full χ^2 procedure used in the Rochester code GOSIA is free of these problems, but sophisticated procedures are necessary to handle the wide range of sensitivities encountered.

Multiple Coulomb excitation is sensitive to both the magnitudes and the relative phases of the matrix elements involved. The procedure used in

the Rochester analysis is to fix the phase of each wave function by defining the sign of one matrix element for each state. The sets of random matrix elements used as starting points in the χ^2 search are arranged to sample all possible signs of interference terms. This is necessary since accurate branching ratio data can lock the search to the initially selected signs for some interference terms. Direct population of unnatural parity states can be orders of magnitude weaker than for adjacent natural parity states because destructive interference occurs for Coulomb excitation of unnatural parity states and because the Coulomb excitation process suppresses such excitation at large scattering angles. Unnatural parity states, such as the 3^+ and 5^+ states of the γ band, usually are seen because of feeding in the γ-ray deexcitation of higher states. The destructive interference in Coulomb excitation usually leads to large errors for the measured E2 matrix elements involving these unnatural parity states.

The computer time required to make a complete model-independent least-squares analysis of Coulomb excitation data depends on the number of states involved, the number of unknowns, the ground-state spin, and the number of experiments. Using the Rochester code GOSIA, a complete analysis of a typical 30-level system with 150 matrix elements will take a minimum of 50 hours of CPU time on a CYBER 175 computer, which is capable of sustaining a computation rate of 2.5×10^6 floating-point instructions per second. For such a case the least-squares minimization will determine those matrix elements most sensitive to the data within one hour of computation, but it takes at least an order of magnitude longer to determine the less sensitive matrix elements. Computing the errors is time consuming, taking on the order of ten hours for 40 matrix elements. Access to more powerful computers is needed to expedite future work in this field.

It is important to verify experimentally the accuracy of the Coulomb excitation methods used. One accurate test of Coulomb excitation is the $B(\mathrm{E2}; 0_1^+ \rightarrow 2_1^+)$ in ^{60}Ni where the Coulomb excitation (50) and resonance fluorescence (51) results agree to $1 \pm 2\%$. The recoil distance technique was used to measure the lifetimes (52) of eight low-lying states in ^{110}Pd to check, in an unambiguous way, the results of earlier Coulomb excitation results (48) analyzed using the GOSIA code. The recoil distance lifetimes are in excellent agreement with the lifetimes calculated from the Coulomb excitation work, i.e. a weighted mean difference of $2.2 \pm 3.5\%$. This confirms that the Coulomb excitation analysis procedure introduces no major systematic errors even for the very complicated case of ^{110}Pd. Agreement at the 5–10% level has been found from comparisons of Coulomb excitation and recoil distance or Doppler-shift attenuation measurements of the $B(\mathrm{E2})$ values for the ground bands of many nuclei (45, 46). Coulomb excitation (53) of ^{7}Li by ^{208}Pb and ^{138}Ba gave a value of the static moment

for the ^{7}Li ground state of $Q_{3/2} = -4.0 \pm 1.1\,e \cdot fm^2$ to be compared with the molecular beam spectroscopy value (54) of $3.66 \pm 0.03\,e \cdot fm^2$; this provides another test of higher order Coulomb excitation. These tests support the validity of the techniques used to analyze Coulomb excitation data.

The importance of the recent advances in the field of Coulomb excitation must not be overlooked. The heavy-ion beams plus the required experimental and analytical techniques now available allow measurement of almost the complete set of E2 matrix elements for the low-lying collective states in a nucleus, i.e. both static moments and the relative signs and magnitudes of off-diagonal matrix elements have been measured for states of low-lying quadrupole collective bands in a wide range of nuclei. The completeness and extent of these large sets of measured E2 matrix elements are sufficient to determine both the centroids and fluctuation widths of the quadrupole shape degrees of freedom for several nuclear states. The completeness is sufficient to allow projection of the quadrupole collective shape degrees of freedom directly from the data, as explained in the next section. Note that the completeness places considerable constraint on the wave functions of states involved and thereby provides a stringent test of models of nuclear structure.

5. EXTRACTION OF COLLECTIVE PARAMETERS FROM E2 MATRIX ELEMENTS

Quadrupole collectivity produces strong correlations of the E2 matrix elements and there are far fewer significant collective variables than there are data. The usual method of comparing a list of the experimental E2 matrix elements with the model values exhibits neither the uniqueness nor the sensitivity of the data to the collective model parameters. In addition such comparisons do not show whether the discrepancies between the experimental and theoretical values reflect a fundamental failure of the model or just deficiencies in the collective model parameters used. Considerably more insight is obtained by projecting the collective degrees of freedom from both the data and the model calculations since they show clearly which collective parameters are determined by the data and how good the collective model description is. This is achieved using rotationally invariant products of multipole operators to relate properties in the principal axis frame directly to those in the laboratory frame (24–26).

The electromagnetic multipole operators are spherical tensors and thus zero-coupled products of such operators can be formed that are rotationally invariant. That is, these products are identical in the instantaneous intrinsic frame and the laboratory frame. Consider the particular case of

the electric quadrupole operator. The electric quadrupole tensor can be rotated into an instantaneous principal axis frame that has only two nonzero quadrupole moments. By analogy with Bohr's parameters (β, γ) we can express the principal axis frame electric moments in terms of two parameters Q, δ, where $\mathrm{E}(2,0) = Q\cos\delta$ and $\mathrm{E}(2,+2) = \mathrm{E}(2,-2) = Q\sin\delta/\sqrt{2}$ and $\mathrm{E}(2,1) = \mathrm{E}(2,-1) = 0$. Zero-coupled products of E2 operators can be evaluated in the principal axis frame, e.g.

$$\{\mathrm{E2}\times\mathrm{E2}\}^0 = (1/\sqrt{5})Q^2$$

$$\{[\mathrm{E2}\times\mathrm{E2}]^2\times\mathrm{E2}\}^0 = -(\sqrt{2/35})Q^3\cos 3\delta$$

$$\{[\mathrm{E2}\times\mathrm{E2}]^0[\mathrm{E2}\times\mathrm{E2}]^0\}^0 = (1/5)Q^4$$

$$\{[\mathrm{E2}\times\mathrm{E2}]^0[(\mathrm{E2}\times\mathrm{E2})^2\times\mathrm{E2}]^0\}^0 = -(\sqrt{2/175})Q^5\cos 3\delta$$

$$\{[\mathrm{E2}\times\mathrm{E2}]^0[\mathrm{E2}\times\mathrm{E2}]^0[\mathrm{E2}\times\mathrm{E2}]^0\}^0 = (\sqrt{1/125})Q^6$$

$$\{[(\mathrm{E2}\times\mathrm{E2})^2\times\mathrm{E2}]^0[\mathrm{E2}\times(\mathrm{E2}\times\mathrm{E2})^2]^0\}^0 = (2/35)Q^6\cos^2 3\delta.$$

It is possible to evaluate expectation values of the E2 invariants in the laboratory frame using experimental E2 matrix elements because the expectation values of the invariants can be written as sums of products of E2 reduced matrix elements by making intermediate state expansions. For example,

$$\langle s|[\mathrm{E2}\times\mathrm{E2}]^0|s\rangle = \frac{(-)^{2s}}{\sqrt{2s+1}}\sum_r \langle s\|\mathrm{E2}\|r\rangle\langle r\|\mathrm{E2}\|s\rangle \begin{pmatrix} 2 & 2 & 0 \\ s & s & r \end{pmatrix}.$$

These intermediate-state expansions can be evaluated using experimental data if the relative signs and magnitudes of the E2 matrix elements are available. Thus, in principle the expectation values for a state s of all the rotationally invariant products of the E2 operator can be evaluated directly using summations of the type shown. These determine directly the distribution of the intrinsic frame electric quadrupole moments, parametrized by Q and δ.

The intrinsic frame electric quadrupole moment distribution for any state can be plotted as contours on a Q-δ plot analogous to the usual β-γ plot, as illustrated in Figure 4. Knowing the values of the various invariants for a state s determines directly the centroids, fluctuation widths, skewnesses, cross-correlation coefficients, etc, describing the distribution in the Q-δ plane of the expectation value of the E2 moment for the state s.

Although this technique of using rotational invariants has been discussed in the context of its application to the collective model, the method is completely model independent and is applicable to any spherical tensor

operator for which the strength is localized to a region amenable to study. The invariants can be evaluated exactly for model calculations and approximately for experimental data; thus they are equivalent to observables. The significance and usefulness of presenting the experimental data in the form of model-independent invariants depends on the degree to which the nuclear properties are correlated by collective degrees of freedom. Model assumptions can be used to relate the Q-δ E2 distributions to the β-γ shape distribution if so desired.

The sensitivity of sum rules to missing strength due to incomplete summation increases markedly with the order and complexity of the invariant. Fortunately, zero-coupled products of four or more operators can be formed with various spins for the intermediate couplings (24, 25). These different intermediate-spin couplings lead to summations over different sets of data. Identities relate these various intermediate-spin zero-coupled products and allow a self-consistency check of the related invariants. For example, using up to sixth-order products leads to four different invariants associated with determining $\cos 3\delta$, three associated with determining $\sigma(Q^2)$, and five associated with determining $\sigma(\cos 3\delta)$. These identities, which depend on the commutation properties of the E2 operators, provide

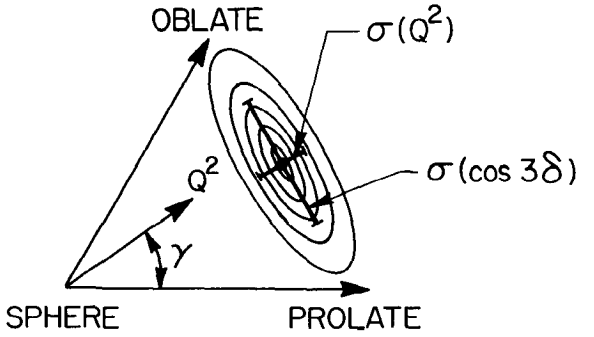

$$Q^2 \begin{cases} \text{Centroid } \langle S|Q^2|S\rangle \\ \text{Width } \sigma(Q^2) = \sqrt{\langle Q^4\rangle - (\langle Q^2\rangle)^2} \end{cases}$$

$$\cos 3\delta \begin{cases} \text{Centroid } \langle S|Q^3 \cos 3\delta|S\rangle \\ \text{Width } \sigma(\cos 3\delta) = \sqrt{\dfrac{\langle Q^6 \cos^2 3\delta\rangle}{\langle Q^6\rangle} - \left(\dfrac{\langle Q^3 \cos 3\delta\rangle}{\langle Q^3\rangle}\right)^2} \end{cases}$$

Figure 4 Distribution plot of the parameters Q^2 and δ required to define the E2 properties in the intrinsic frame. All possible E2 moments are defined by the region $Q \geq 0$ and $0° \leq \delta \leq 60°$.

a direct test of completeness and convergence of the invariants. Note that the E2 operators used in some collective models, such as the Interacting Boson Model (55), have unusual commutation properties and as such do not satisfy these identities. The completeness of the set of E2 properties measured in typical Coulomb excitation experiments is sufficient to determine, with reasonable precision, the centroids for about a dozen states and the widths for the lowest two or three states.

The low-lying levels contain only $\sim 10\%$ of the E2 energy-weighted sum-rule strength in nuclei. The giant E2 resonance, which we have ignored so far, could contain the other 90% of this strength. Fortunately, we are considering non-energy-weighted sum rules. About 90–95% of the non-energy-weighted E2 strength is in the lowest few states for the strongly deformed nuclei and greater than 70% for any nucleus for which a collective model description would be considered reasonable. The high-lying E2 strength obviously is nonnegligible. However, the separation of the E2 strength into two quite distinct and separate collective modes is important. Thus in a collective picture we have a high-frequency collective mode, corresponding to the giant resonance, superimposed on a low-frequency collective mode. Most collective models implicitly assume only the low-frequency mode. The same result of effectively averaging over the high-frequency mode may be achieved by including only the low-lying strength in evaluating the invariants. Of course this assumption is only reasonable if the two modes are distinct and weakly coupled and if the high-frequency oscillation about the low-frequency shape is relatively small.

The recent advances in the field of Coulomb excitation make it possible to determine all the E2 matrix elements required to apply this model-independent method and thereby express a wealth of data in a form that exhibits clearly the extent to which the data are correlated by collectivity. Tests of collective models should employ comparison with data using both the rotational invariants and the individual matrix elements. The rotational invariants provide the most insight into the underlying collective correlations at the expense of some loss in precision due to incomplete summation. Models selected to have reasonable values of the rotational invariants can be refined by making a fit to the individual matrix elements; this makes the quantitative comparison with data more precise.

6. QUADRUPOLE COLLECTIVITY IN STRONGLY DEFORMED NUCLEI

6.1 *Ground-State Rotational Band*

Coulomb excitation has been used extensively to populate states up to spins as high as $30\hbar$ in the ground rotational bands in many strongly

deformed rare earth and actinide nuclei. In-band $B(E2)$ values have been measured for many of these nuclei using either Coulomb excitation cross sections or by employing the recoil distance or Doppler-shift attenuation methods in conjunction with Coulomb excitation to measure lifetimes of excited states. Examples of such work employing the heaviest ions are ^{156}Gd (56), ^{156,162,164}Dy (57–59), ^{164,168}Er (47, 60, 61), ^{170,172,174,176}Yb (46, 62), ^{182,184,186}W (42, 63), ^{230,232}Th (45, 64–66), ^{234,236,238}U (65, 67), ^{242,244}Pu (68), and ^{248}Cm (69, 70).

A surprising result, discovered 10 years ago (45, 46) and confirmed by recent work, is that for strongly deformed nuclei the measured ground band $B(E2)$ values obey the simple rigid spheroidal-rotor relation with remarkable accuracy except at band intersections or for nuclei adjacent to shape transitions. Figure 5 shows a typical example that is a composite of measurements of the $B(E2)$ values for the ground band of ^{232}Th derived

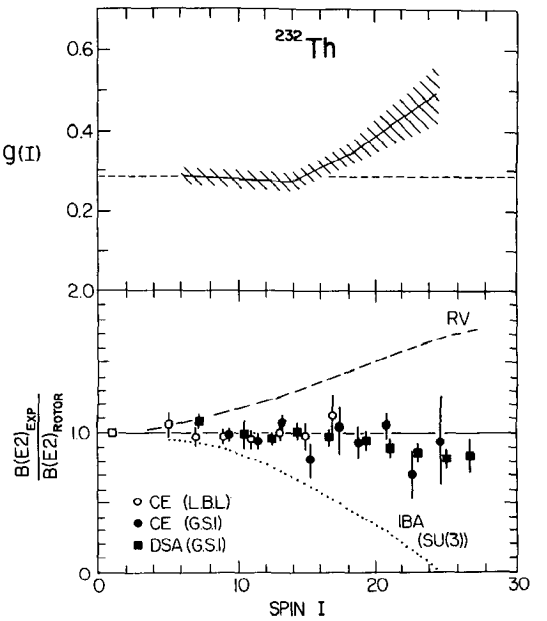

Figure 5 The lower plot shows the measured $B[E2; (I+1) \rightarrow (I-1)]$ values (45, 65, 66) normalized to the axially symmetric rigid rotor value for the ground band of ^{232}Th. The IBA calculation assumes 12 bosons outside a ^{208}Pb core and the SU(3) limit. The Rotation-Vibration Model values are those that result from attributing change in the ground band moment of inertia to centrifugal stretching. The upper plot shows the measured g-factors for the ground band states (75). The cross-hatched region reflects the experimental uncertainty while the dashed line shows the value derived if the g-factors are assumed to be constant.

from recoil distance, Doppler-shift attenuation, and Coulomb excitation yields (45) measured at Berkeley and from Coulomb excitation yield (65) and Doppler-shift attenuation (66) measurements made at GSI. The B(E2) values from the lifetime and Coulomb excitation yield measurements are in excellent agreement. The intrinsic transition quadrupole moment, and consequently the magnitude of the deformation β^2, are remarkably constant up to spin 28 $\hbar$ in ^{232}Th. Heavy-ion Coulomb excitation data also determine the static electric quadrupole moments as well as the transition matrix elements. The latest analyses of data for ^{168}Er (61) and ^{248}Cm (70) show that the static quadrupole moments also obey the rigid prolate spheroidal-rotor relation as illustrated in Figure 7, which implies that the asymmetry parameter $\gamma \approx 9°$ for ^{168}Er.

The moment of inertia in strongly deformed nuclei below band intersections usually exhibits a smooth ω dependence of the form $\mathcal{I}(\omega) = \mathcal{I}_0 + \mathcal{I}_1\omega^2$. This ω dependence can be ascribed to either a weakening of the pairing correlations at higher spins due to the Coriolis force, i.e. Coriolis anti-pairing, or to shape changes due to centrifugal stretching. The latter explanation is inconsistent with the remarkable constancy of the transition quadrupole moments for strongly deformed nuclei as illustrated by calculations within the rotation-vibration model (curve RV in Figure 5). Thus Coriolis anti-pairing appears to be the reason for the spin dependence of the moment of inertia.

The Interacting Boson Model (55) is reasonably successful in correlating collective behavior for low-spin states in deformed nuclei. However, the limited number of $L = 0$ and 2 bosons employed leads to band termination and concomitant retardation of the B(E2) values, which is in conflict with the B(E2) data for ^{232}Th and for many other strongly deformed rare earth and actinide nuclei. These results indicate that higher angular momentum bosons as well as excitation into the next valence shell need to be included in this model to account for the properties of higher spin states.

6.2 *Band Intersections in the Yrast Sequence*

One stimulus for this work was the discovery of the backbending phenomenon (71) in strongly deformed rare earth nuclei, that is, a discontinuity in the moment of inertia of the ground band caused by an intersection of the ground rotational band with a second rotational band having a larger moment of inertia. This intersection occurs at about spin 16 in rare earth nuclei and spin 22 in actinide nuclei. The structure of the band intersecting the ground band usually is dominated by a rotation-aligned (72) two-quasiparticle configuration involving high-j nucleons, i.e. the angular momenta are aligned along the rotation axis by the Coriolis force. Coulomb excitation up through the band intersection was first observed for

^{164}Er and ^{170}Yb (60, 62) using ^{136}Xe ions from the SuperHILAC at Berkeley. The GSI group have made an extensive study of the yrast sequence of states for several actinide nuclei (17, 73). Coulomb excitation is the only viable method for populating high-spin states in such nuclei because fusion reactions primarily lead to fission. Of these nuclei, only ^{244}Pu exhibits, at spin 22, a pronounced discontinuity or backbend in the effective moment of inertia (68); ^{230,232}Th, ^{234,236,238}U, ^{242}Pu, and ^{248}Cm exhibit a smoothly increasing moment of inertia with spin. The energy level spectra and the B(E2) values can be understood in terms of the intersection of two rotational bands (73).

Magnetic moments probe the single-particle degrees of freedom in contrast to the E2 properties, which probe the collective degrees of freedom. Coulomb excitation has been used, in conjunction with the transient field method, to measure g-factors of excited states through the backbend region for ^{160}Dy and ^{170,174}Yb (74), ^{232}Th and ^{232}U (75), as well as ^{158}Dy (76). The measured g-factors for ^{232}Th, shown in Figure 5, are constant up to spin 14, consistent with a pure ground-state rotational band, but they increase markedly through the band intersection region, centered at spin 22, which provides convincing evidence that the structure of the band intersecting the ground band is dominated by a rotation-aligned pair of protons in the $i_{13/2}$ intruder orbit and not neutrons in the $j_{15/2}$ intruder orbit, which also lies in the vicinity of the Fermi surface. The measured g-factors for ^{158,160}Dy and ^{170,174}Yb decrease markedly through the backbend region, which implies that the structure of the intersecting band is dominated by the intruder $i_{13/2}$ two-quasineutron configuration in these nuclei.

In their ground states, the odd neutron in ^{235}U occupies the [743 7/2$^-$] $j_{15/2}$ neutron intruder shell while the odd proton in ^{237}Np occupies the [642 5/2$^+$] $i_{13/2}$ proton intruder shell. The spectra of these odd-A nuclei provide a means of identifying the importance of these two high-j intruder orbits in the structure of the intersecting bands responsible for backbending in adjacent even-A nuclei. At moderate spins the observed spectra in these nuclei exhibit the relative ease of rotation alignment of the valence high-j nucleon. At higher spin the unpaired nucleon blocks further alignment within its own subshell and thus can modify the backbending behavior. These two odd-A nuclei have been studied by Coulomb excitation and states up to spin 57/2 were identified (77), as shown in Figure 6. The ^{237}Np spectrum exhibits the clear signature of a rotation-aligned proton that also blocks the onset of the band intersection relative to ^{238}U. In contrast, the spectrum of ^{235}U exhibits less rotation alignment of the odd neutron at lower spins and the band intersection is not perturbed. These results show the dominance of the $i_{13/2}$ proton orbit in the structure of the band

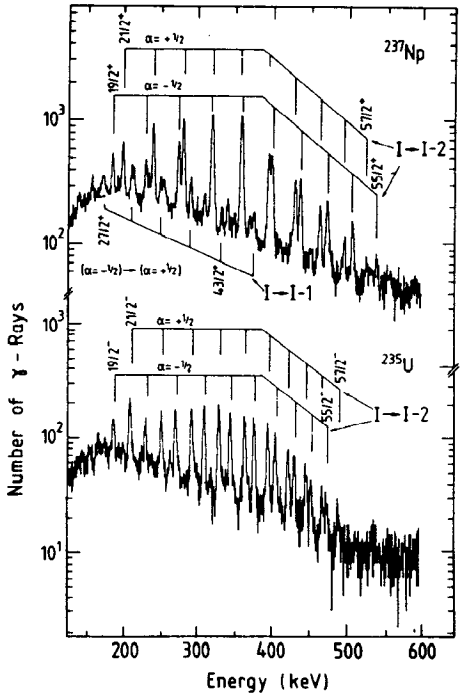

Figure 6 Gamma spectra resulting from Coulomb excitation (77) of ^{237}Np and ^{235}U by 5.3 MeV per nucleon ^{208}Pb in coincidence with ions at center-of-mass scattering angles between 96° and 145°.

intersecting the ground band in these actinide nuclei, supporting similar conclusions drawn from the *g*-factor measurements.

The high selectivity of Coulomb excitation results in clean spectra for odd-*A* nuclei (Figure 6) and for the odd-odd nucleus ^{176}Lu, where the γ-ray spectrum (78) is dominated by the decay of a rotational band seen to spin 21^-, which is based on the 7^- ground state. Current Coulomb excitation studies (43) of strongly deformed odd-*A* nuclei are measuring the E2 and M1 properties to probe both collective and single-particle degrees of freedom in order to investigate Coriolis effects in nuclei.

6.3 *E2 Properties of Non-yrast Rotational Bands*

The properties of non-yrast collective bands are a more sensitive probe of collective models than are the properties of the yrast states. An extensive study (79) of ^{168}Er by thermal neutron capture identified 20 low-*K* rotational bands. Coulomb excitation of ^{168}Er by ^{40}Ca, ^{58}Ni, and ^{208}Pb ions has been used (61) to measure 54 E2 matrix elements involving the ground

and γ bands to complement the rather complete data set of level energies. Figure 7 summarizes the transition and diagonal matrix elements for the ground and γ bands. The predictions of the rigid spheroidal rotor model, the asymmetric rigid rotor model (not shown), and the Interacting Boson Model all are in good agreement with the data shown in Figure 7. The interband E2 matrix elements between the ground and γ bands are more sensitive to the model predictions. The asymmetric rigid rotor using $\gamma = 9°$ reproduces the data well although these data are relatively insensitive to the γ softness about such a small centroid of $\gamma = 9°$. The Interacting Boson Model predictions deviate somewhat from these data.

The rotational invariants have been evaluated using the measured E2 properties of ^{168}Er and the centroids are presented in Figure 8. The magnitude of $\langle Q^2 \rangle$ in both bands is spin independent, and averages $\sim$6.0 (e.b)^2 for the ground band and $\sim$7.0 (e.b)^2 for the gamma band. The complete spin independence of these data implies the existence of strong correlations for the E2 properties, which is consistent with the rotation-like quadrupole behavior of individual E2 matrix elements. A similar

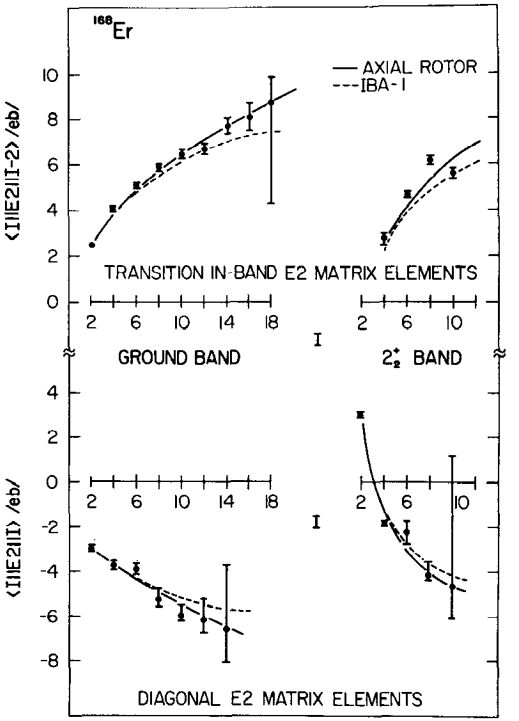

Figure 7 The in-band E2 matrix elements for the ground and gamma bands of ^{168}Er (61).

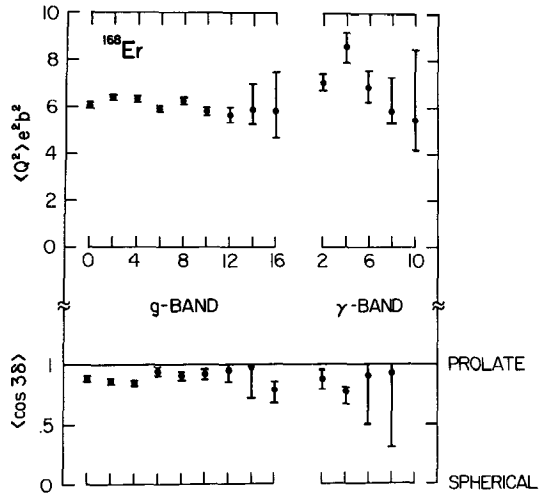

Figure 8 Centroids for the magnitude and asymmetry of the intrinsic frame E2 properties of the states of the ground and gamma bands of ^{168}Er.

feature can be seen in the case of the asymmetry $\langle \cos 3\delta \rangle$ for the ground band states, which is constant ~ 0.9, i.e. $\delta \approx 9°$. This corresponds to an almost pure prolate shape. The widths $\sigma(Q^2)$ and $\sigma(\cos 3\delta)$, not shown, suggest a relative "stiffness" in both the magnitude Q^2 and an asymmetry δ for ground band states in ^{168}Er. The individual E2 matrix elements and the rotational invariants for the ground and γ bands in ^{168}Er all are consistent with rotation of a quadrupole deformed rotor with asymmetry centroid of $\gamma \approx 9°$, which demonstrates that quadrupole collectivity is the dominating feature for the states in these bands.

The E2 properties of the β, γ, and octupole bands in ^{230,232}Th have been studied by Coulomb excitation with ^{32}S ions (80, 81) and B(E2) ratios measured for these bands. The Bohr & Mottelson model (82) of weakly interacting rotational bands reproduces the data well. Moreover, the interaction between the β and γ bands appears to be much weaker than predicted by calculations using the Rotation-Vibration Model or the Interacting Boson Model.

7. SHAPE TRANSITIONAL NUCLEI

7.1 *Prolate-Oblate Shape Transition in Os and Pt Nuclei*

Quadrupole collectivity is a prominent feature of shape transitional nuclei, such as the even-A platinum and osmium nuclei for which the $B(\mathrm{E2}; 0^+ \rightarrow 2^+)$ values are 40 to 90 single-particle units. Coulomb excitation measure-

ments (14, 83, 84) of the static quadrupole moments of the 2_1^+ have shown that a prolate-to-oblate shape transition occurs in the osmium-platinum nuclei, but there has been no reliable determination of the fluctuation widths of the quadrupole shape parameters β and γ. Various collective models, ranging from the Rigid Triaxial Rotor (85) to the Interacting Boson Model (55), have been used to describe these nuclei but the available data were insufficient to differentiate between the competing models.

Coulomb excitation of ^{186,188,190,192}Os and ^{194}Pt by ^{40}Ca, ^{58}Ni, ^{136}Xe, and ^{208}Pb ions (37, 38) populated levels up to spin 12^+ of the ground band, 10^+ of the γ band, and 6^+ of the 4^+ band in most of the nuclei studied. Figure 9 shows a typical level scheme resulting from this work. The magnitudes and observable signs of between 30 and 38 transition and diagonal matrix elements were determined, with reasonably small errors, for each of the five nuclei. These include, in most nuclei, static electric quadrupole

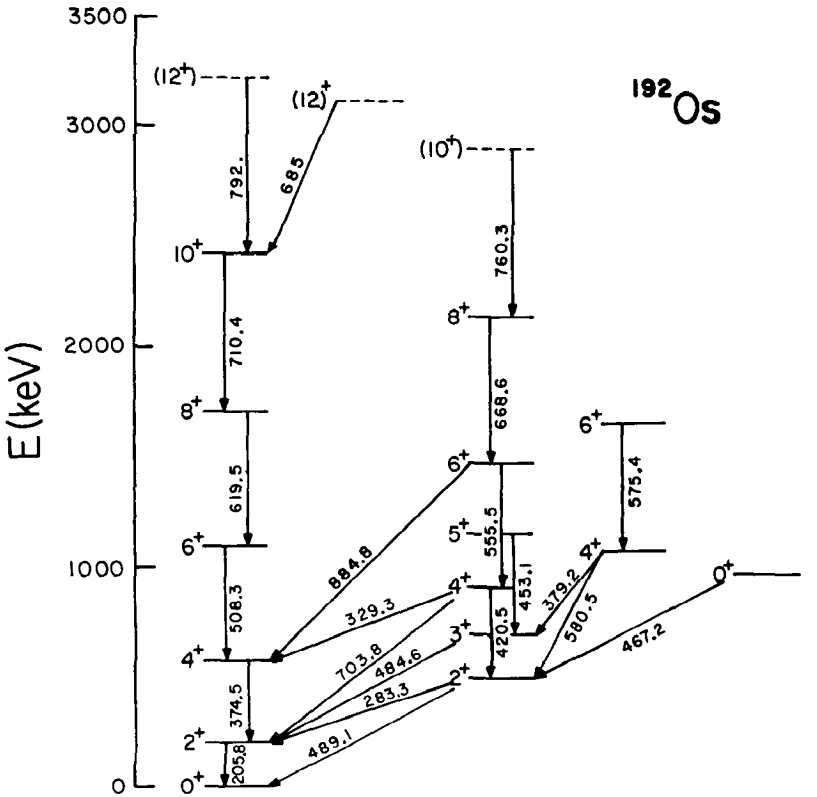

Figure 9 Level scheme of ^{192}Os derived from Coulomb excitation (37, 38).

moments of members of the ground band to spin 10^+, the γ band to spin 8^+, and the 4^+ band head.

The rotational invariants were used to project the principal axis frame E2 properties from the Coulomb excitation data to test the validity of collective model descriptions for these nuclei. Figure 10 shows that the centroids $\langle Q^2 \rangle$ and $\langle \cos 3\delta \rangle$ are almost constant for the excited states of ^{192}Os, which implies a strong correlation of the E2 properties consistent with rotation-like quadrupole collective motion. Similar results were obtained for ^{186,188,190}Os and ^{194}Pt. The expectation values of both the centroids and widths for the ground states of these nuclei are shown in Figure 11. The centroids $\langle Q^2 \rangle$ illustrate the gradual reduction in deformation with increasing mass while the centroids $\langle \cos 3\delta \rangle$ correspond to triaxial deformation throughout a prolate-to-oblate shape transition. The agreement between the several independent measures of $\cos 3\delta$ and the widths illustrates that reasonable convergence is obtained for the ground states. The mass dependence of the softness in asymmetry (δ) and the moderate stiffness in magnitude (Q^2) of the quadrupole deformation are apparent. These results demonstrate that the E2 data for the low-lying levels are correlated well using only quadrupole collective degrees of freedom throughout a prolate-to-oblate shape transition.

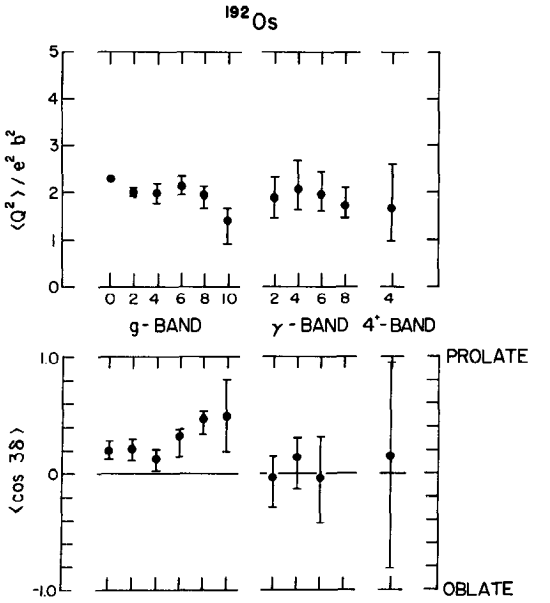

Figure 10 Centroids Q^2 and $\cos 3\delta$ versus spin for the ground band, γ band, and 4^+ band head in ^{192}Os.

The ~200 measured E2 matrix elements were compared with the predictions of two extreme collective models—the Rigid Asymmetric Model and model calculations employing the complete Bohr collective Hamiltonian with γ-soft shapes for the potential energy—to test the sensitivity of individual data to the γ softness. In addition, the data were compared with the Interacting Boson Model predictions using parameters fitted to the level spectra. The γ-soft potentials are more successful in reproducing the data but all three models reproduce only part of the data. Better model calculations are required to make a meaningful fit to the individual matrix elements.

Coulomb excitation studies (86, 87) determined the E2 properties of the ground and γ bands of ^{196}Pt; a comparison with similar model calculations leads to the same conclusion that triaxial γ-soft collective models best reproduce the data. Similar work (88) on ^{198,200}Hg populated only the yrast band, which is insensitive to the γ softness. The B(E2) values in the ground

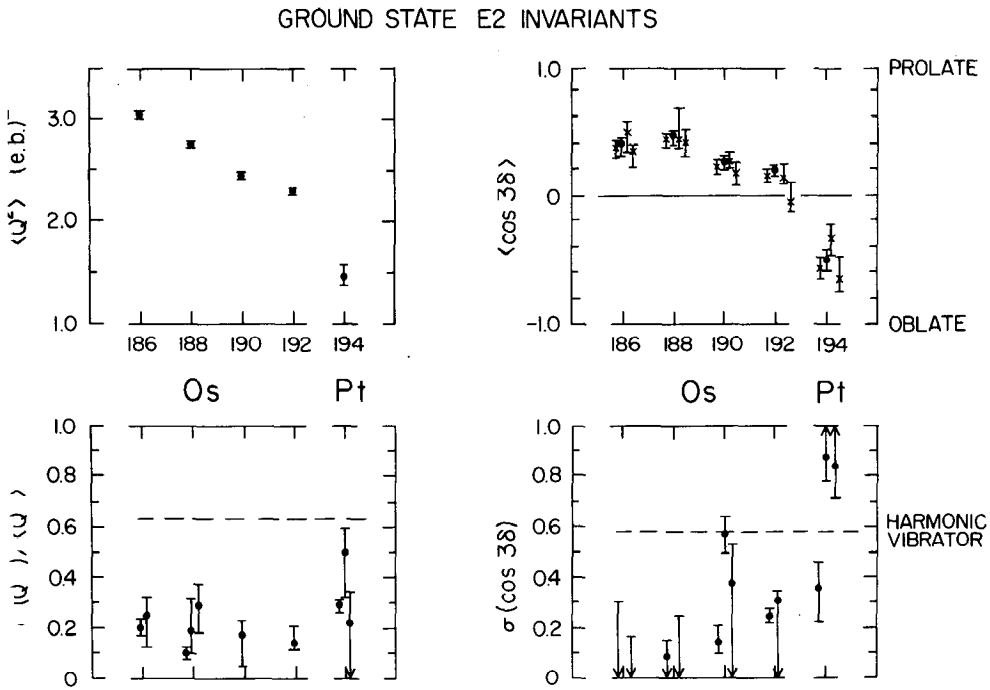

Figure 11 Centroids (*upper*) and fluctuation widths (*lower*) for the magnitude and asymmetry of the intrinsic frame E2 properties of the ground states of ^{186}Os, ^{188}Os, ^{190}Os, ^{192}Os, and ^{194}Pt. Four values of cos 3δ are shown for each state; one derived using the third-order invariant (*solid point*) and three from the fifth-order invariants (*crosses*).

band of ^{198}Hg follow the rigid rotor relation except at the band intersection, where the E2 strength is split between two 8^+ states.

7.2 *Shape Coexistence in Medium-Mass Nuclei*

For many years the low-lying states of the even-mass ruthenium, palladium, and cadmium nuclei have been viewed as having a structure with an underlying vibrational character. For example, a closely spaced "two-phonon" 0^+, 2^+, 4^+ triplet exists in ^{110}Pd and the $B(E2; 0_1^+ \rightarrow 2_1^+)$ is 55 single-particle units. The vibrational model interpretation is based on relatively few experimental data, therefore the collective properties of ^{110}Pd were investigated by Coulomb excitation using ^{16}O, ^{58}Ni, and ^{208}Pb ions (48, 52). The analysis determined the values of 89 E2 matrix elements with sufficient accuracy to make a meaningful comparison with model predictions. The level spectrum from ^{110}Pd derived from this work is shown in Figure 12. The low-lying levels group into four rotational bands, in contrast to earlier vibrational model interpretations. Backbending behavior is also manifest in ^{110}Pd. The in-band transition and diagonal E2 matrix elements for these bands have a rotational character that for the ground and quasi-gamma bands corresponds to $Q_0 = 2.85$ eb and $\delta = 18°$, while the 0_2^+ band has $Q_0 = 3.74$ eb and $\delta = 18°$, i.e. 31% more deformed

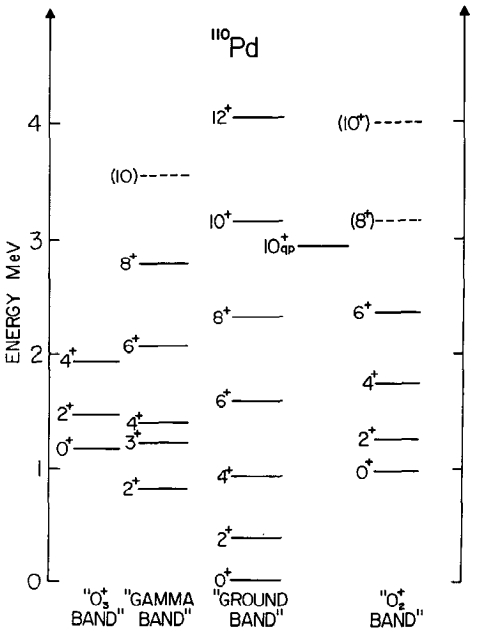

Figure 12 The level spectrum of ^{110}Pd derived from Coulomb excitation work (48).

than the ground or γ bands. Clearly it is fortuitous that the 0_2^+ state appears to be a member of a two-phonon triplet; the 0_3^+ state behaves more like the two-phonon 0^+ state.

Figure 13 shows the E2 properties in the principal axis frame that were derived from the measured E2 matrix elements using the rotational invariants. Note that the expectation values $\langle Q^2 \rangle$ for the ground band increase from $0.8(\text{eb})^2$, i.e. $\beta_2 \approx 0.25$, for the 0_1^+ state until they saturate at $\sim 1.3(\text{eb})^2$ ($\beta_2 \approx 0.32$) for the 4_1^+ and higher states in the ground band. The band head of the 0_2^+ band has a value of $\langle Q^2 \rangle = 1.6(\text{eb})^2$ ($\beta_2 \approx 0.35$), which is larger than for the ground state. The quadrupole asymmetry, as measured by $\langle \cos 3\delta \rangle$, indicates prolate shapes for the ground, gamma, and 0_2^+ bands while the 0_3^+ band is more triaxial. All bands show large softness in both $\langle Q^2 \rangle$ and $\cos 3\delta$. In summary, the low-lying E2 properties

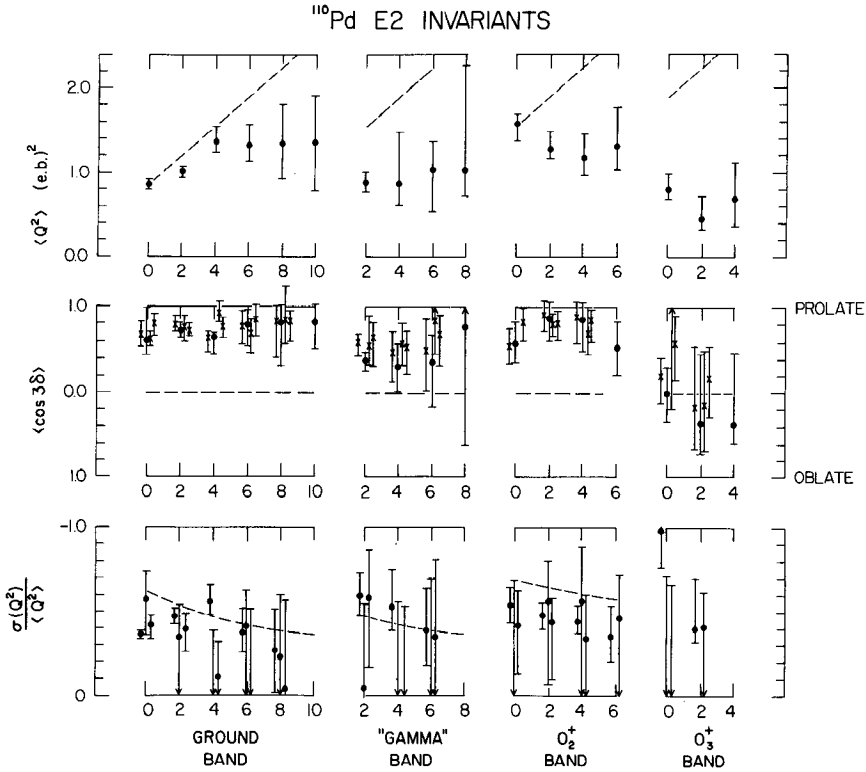

Figure 13 Centroids of Q^2 and $\cos 3\delta$ and the fluctuation width $\sigma\langle Q^2 \rangle$ for the states of the ground, gamma, 0_2^+, and 0_3^+ bands in ^{110}Pd. The dashed lines represent predictions of the harmonic vibrator model. Four values of $\cos 3\delta$ are shown for each state; one derived from the third-order invariant (*solid point*) and three from the fifth-order invariants (*crosses*).

of ^{110}Pd are correlated well using macroscopic quadrupole collective degrees of freedom, and both spin-dependent shapes and shape coexistence are manifested. Both the Interacting Boson Model and the Boson Expansion Theory (89) are able to reproduce the general features of the E2 properties of the ground and γ bands, but the 0_2^+ band is an intruder band not contained in the model calculations.

Traditionally ^{114}Cd has been considered to have features characteristic of a slightly anharmonic vibrator. However, intruding 0^+ and 2^+ states of unknown origin occur among the two-phonon triplet of states in ^{114}Cd. This quintuplet of states has been investigated by Coulomb excitation with ^{16}O, ^{40}Ca, ^{58}Ni, and ^{208}Pb ions and many E2 matrix elements have been determined (90). The 19 E2 matrix elements involved in the excitation of the quintuplet can be understood in terms of a strongly deformed intruder rotational band similar to that in ^{110}Pd.

The nucleus ^{104}Ru has been Coulomb excited using both the Berkeley and the GSI heavy-ion accelerators (34, 91, 92). It was necessary to perform γ-γ coincidence measurements (91) to identify the upper members of the ground and γ bands where band intersections perturb the rotational band structure. The GSI work extracted 25 E2 matrix elements from their data. The results are similar in most respects to the earlier work on ^{110}Pd discussed above. The E2 properties can be understood in terms of triaxial collective models having appreciable fluctuations in the β and γ degrees of freedom. That is, the ground and γ bands are observed to have a deformation of about $\beta = 0.23$ and $\gamma = 25°$ while the 0_2^+ state is the band head of an intruder rotational band that has a deformation similar to the ground band, i.e. it is not as deformed as the intruder 0^+ band in either ^{110}Pd or ^{114}Cd.

The nucleus ^{72}Ge has been Coulomb excited by ^{208}Pb, ^{58}Ni, and ^{16}O ions; 21 matrix elements involving the 7 lowest states were determined (39). These results are consistent with a soft triaxial quadrupole structure ($\beta = 0.3, \gamma = 28.5$), perturbed by an isolated, presumed spherical, intruder 0^+ state. Projectile Coulomb excitation of ^{82}Kr by a ^{208}Pb target (93) determined 13 transition E2 matrix elements that are consistent with triaxial quadrupole deformation similar in some respects to that seen in ^{72}Ge.

In summary the E2 data in all these nuclei are correlated surprisingly well using collective models that have fluctuating triaxial quadrupole deformed shapes, and in some cases, include coexistence of differently shaped configurations.

8. PROSPECTS FOR THE FUTURE

After three decades of work in this field it is possible finally to utilize the powerful technique of Coulomb excitation to measure almost the complete

set of E2 matrix elements for low-lying states in nuclei. The next few years should see exploitation of this technique to study further the limits of validity of the collective model, the role of symmetries in collective motion, shape transitions, shape coexistence, octupole deformation, and the interplay of single-particle and collective degrees of freedom in nuclear structure. Methods may be developed to exploit the completeness of the data sets now being measured to determine directly the model content of wave functions of low-lying states without resorting to large model calculations, which obfuscate model interpretations of nuclear structure.

The experimental and analytical techniques have reached the stage where the study of odd-A nuclei is practical. Both M1 and E2 matrix elements result from such studies, which probe simultaneously both the single-particle and collective degrees of freedom. Current work on odd-A nuclei is focussed on the attenuation of Coriolis effects in rotational bands and the validity of the Interacting Boson-Fermion Model (55) of nuclear structure.

Coulomb excitation is restricted to nuclear species available as targets or projectiles. Stable nuclei are not available to address some of the interesting problems in nuclear structure, such as the question of whether stable octupole deformation occurs in nuclei. Radioactive targets are being used to extend the range of nuclei available to Coulomb excitation to probe such questions, but the range of available targets is limited. One exciting possibility for the future is the use of radioactive secondary beams, which may become available in the future. The large Coulomb excitation cross sections make such experiments feasible and extend considerably the range of nuclei available for study. The considerable increase in scope of such experiments could have a profound influence on the study of nuclear structure.

Coulomb excitation using bombarding energies below the safe energy criterion, 4.5 MeV per nucleon, results in an adiabatic cutoff limiting excitation to within 2 MeV of the yrast sequence of states. However, pure Coulomb excitation dominates the cross section forward of the grazing angle for heavy-ion scattering above the Coulomb barrier. For a given distance of closest approach the limiting excitation energy increases with projectile velocity. Thus, increasing the bombarding energy to 20 MeV per nucleon allows excitation of states within 4 MeV of the yrast sequence, albeit with reduced multistep excitation, which reduces the maximum-spin states excited, while even the giant Eλ resonances are excited with large probability for bombarding energies above 60 MeV per nucleon. At relativistic energies, the excitation probability becomes almost independent of excitation energy (94). Use of such high-energy heavy ions opens up the possibility of using the high selectivity of Coulomb excitation to locate and study both giant resonances and exotic collective structures that may exist at high excitation energies in nuclei.

9. CONCLUSIONS

Considerable advances made recently in the field of Coulomb excitation make it feasible for the first time to measure almost the complete set of E2 matrix elements involving the lowest 20–30 collective states in nuclei. The extent and completeness of the E2 data now being measured are sufficient to determine directly the centroids and fluctuation widths of the E2 properties in the principal axis frame for several low-lying collective states. These show clearly the extent to which the data are correlated due to collectivity, adding a new dimension to the study of quadrupole collectivity in nuclei.

These new techniques are being applied to a wide range of nuclei. The examples given show that the measured E2 properties are correlated very well using quadrupole collective degrees of freedom in both strongly deformed and shape transitional nuclei. Moreover, the results determine the quadrupole shapes occurring through shape transitions and shape coexistence as well as illuminating the interplay of single-particle and collective degrees of freedom in nuclear structure. Collective models employing either geometric or boson degrees of freedom are able to reproduce the general trends of the data but available model calculations fail to give a detailed fit to the large sets of E2 data. More refined collective model calculations are needed.

It is anticipated that the recent developments will ensure that Coulomb excitation will continue to play a prominent role in the study of single-particle and collective degrees of freedom in nuclear structure.

ACKNOWLEDGMENTS

The author wishes to thank his many collaborators, especially Drs. T. Czosnyka, L. Hasselgren, B. Kotlinski, and C. Y. Wu, who played a key role in some of the developments described in this review.

Literature Cited

1. Bohr, A. *Mat. Fys. Medd. Dan. Vid. Selsk.*, Vol. 26, No. 14 (1952)
2. Bohr, A., Mottelson, B. R. *Mat. Fys. Medd. Dan. Vid. Selsk.*, Vol. 27, No. 16 (1953)
3. Mottelson, B. See Ref. 9, pp. 11–14
4. McClelland, C. I., Goodman, C. *Phys. Rev.* 91:760 (1953)
5. Huus, T., Zupancic, C. *Mat. Fys. Medd. Dan. Vid. Selsk.* 28:No. 1 (1953)
6. Alder, K., Bohr, A., Huus, T., Mottelson, B. R., Winther, A. *Rev. Mod. Phys.* 28:432 (1956)
7. Bohr, N. *Philos. Mag.* 6:25 (1913)
8. Biedenharn, L. C., Brussaard, P. J. *Coulomb Excitation.* Oxford: Clarendon (1965)
9. Alder, K., Winther, A. *Coulomb Excitation.* New York: Academic (1966)
10. Alder, K., Winther, A. *Electromagnetic Excitation, Theory of Coulomb Excitation with Heavy Ions.* Amsterdam: North-Holland (1975)
11. Stelson, P. H., McGowan, F. K. *Ann. Rev. Nucl. Sci.* 13:163 (1963)
12. McGowan, F. K., Stelson, P. H. *Nuclear*

Spectroscopy and Reactions, C, ed. J. Cerny. New York: Academic (1974)
13. Newton, J. O. *The Electromagnetic Interaction in Nuclear Spectroscopy*, ed. W. D. Hamilton, pp. 237–82. Amsterdam: North-Holland (1975)
14. Cline, D. *Lect. Notes Phys.*, Vol. 92, *Nuclear Interactions*, ed. R. A. Robson, pp. 39–55. New York: Springer-Verlag (1978)
15. Cline, D. *Proc. Int. Conf. Interacting Bose-Fermi Systems in Nuclei*, ed. F. Iachello, pp. 241–55. New York: Plenum (1980)
16. de Boer, J. *Treatise on Heavy-Ion Science*, 1: 293–352. New York: Plenum (1984)
17. Elze, Th. W. *Proc. Niels Bohr Cent. Symp. on Semiclassical Descriptions of Atomic and Nuclear Collisions*, ed. J. Bang, J. de Boer, pp. 101–18. New York: Elsevier Science (1985)
18. Cline, D. *Proc. Niels Bohr Centennial Symp. on Nuclear Structure*, ed. R. Broglia, G. B. Hagemann, B. Herskind, pp. 313–26. New York: Elsevier Science (1985)
19. Newton, J. O., Stephens, F. S. *Phys. Rev. Lett.* 1: 63 (1958)
20. Stephens, F. S., Diamond, R. M., Perlman, I. *Phys. Rev. Lett.* 3: 435 (1959)
21. Winther, A., de Boer, J. See Ref. 9, pp. 303–74
22. Czosnyka, T., Cline, D., Wu, C. Y. *Bull. Am. Phys. Soc.* 28: 745 (1983)
23. Grein, H., Emling, H., Stachel, J. *Scientific Report 1983, GSI-84-1*, p. 272. Darmstadt: GSI (1984)
24. Cline, D., *Proc. of the Orsay Colloquium on Intermediate Nuclei*, ed. R. Foucher, N. Perrin, M. Veneroni, pp. 4–34. Orsay: Inst. Phys. Nucl. (1971)
25. Cline, D., Flaum, C. *Proc. of the Int. Conf. on Nucl. Struct. Studies using Electron Scattering and Photoreaction, Sendai 1972*, ed. K. Shoda, H. Ui, 5: 61–82. Sendai: Tohoku Univ. (1972)
26. Kumar, K. *Phys. Rev. Lett.* 28: 249 (1972)
27. Cline, D., Gertzman, H. S., Gove, H. E., Lesser, P. M. S., Schwartz, J. J. *Nucl. Phys.* A133: 445 (1969)
28. Lesser, P. M. S., Cline, D., Goode, P., Horoshko, R. N. *Nucl. Phys.* A190: 597 (1972)
29. Cline, D. *Proc. Int. Conf. on the Physics of Medium-Light Nuclei*, ed. P. Blasi, R. A. Ricci, p. 89. Bologna: Editrice Compositori (1978)
30. Vold, P. B., Cline, D., Russo, P., Sprinkle, J. K., Scharenberg, R. P., Mitchell, R. F. *Phys. Rev. Lett.* 39: 325 (1977)
31. Tolsma, L. D. *Phys. Rev.* C20: 592 (1979)
32. Rhoades-Brown, M., MacFarlane, M. H., Pieper, S. C. *Phys. Rev.* C21: 2417 (1980)
33. Bohr, N. *Mat. Fys. Medd. Dan. Vid. Selsk.* 18: No. 8 (1948)
34. Stachel, J., Kaffrell, N., Grosse, E., Emling, H., Folger, H., et al. *Nucl. Phys.* A383: 429 (1982)
35. Abragam, A., Pound, R. V. *Phys. Rev.* 92: 943 (1953)
36. Brenn, R., Spehl, H., Weckherlin, A., Doubt, H. A., Van Middelkoop, G. Z. *Phys.*, A281: 219 (1977)
37. Wu, C. Y. PhD thesis. Univ. Rochester (1983)
38. Wu, C. Y., Cline, D., Czosnyka, T., Bäcklin, A., Chaki, T. K., et al. Submitted to *Nucl. Phys.* (1986)
39. Kotlinski, B., Czosnyka, T., Bäcklin, A., Cline, D., Wu, C. Y., et al. *Bull. Am. Phys. Soc.* 28: 686 (1983)
40. Cline, D., Kotlinski, B. *Univ. Rochester Nucl. Struct. Res. Lab. 1982–1983 Biennial Rep.* pp. 363–65 (1984)
41. Kotlinski, B. PhD thesis. Univ. Rochester (1984)
42. Wu, C. Y., Cline, D., Czosnyka, T., Kavka, A., Kernan, W. J., et al. *Univ. Rochester Nucl. Struct. Res. Lab. 1984–1985 Biennial Rep.* (1986)
43. Cline, D., Lee, I. Y., Stephens, F. S., Aleonard, M. M., Deleplanque, M. A. See Ref. 14, p. 42 (1978)
44. Lee, I. Y., Cline, D., Simon, R. S., Butler, P. A., Colombani, P., et al. *Phys. Rev. Lett.* 37: 39 (1976)
45. Guidry, M. W., Butler, P. A., Colombani, P., Lee, I. Y., Ward, D., et al. *Nucl. Phys.* A266: 228 (1976)
46. Ward, D., Colombani, P., Lee, I. Y., Butler, P. A., Simon, R. S., et al. *Nucl. Phys.* A266: 194–214 (1976)
47. Yates, S. W., Lee, I. Y., Johnson, N. R., Eichler, E., et al. *Phys. Rev.* C21: 2366 (1980)
48. Hasselgren, L., Cline, D. *Proc. of the Int. Conf. on Interacting Bose-Fermi Systems in Nuclei*, ed. F. Iachello, pp. 59–64. New York: Plenum (1980)
49. Cline, D., Lesser, P. M. S. *Nucl. Instrum. Methods* 82: 291 (1970)
50. Lesser, P. M. S., Cline, D., Cline, C. K., Bahnsen, A. *Nucl. Phys.* A223: 563 (1974)
51. Metzger, F. R. *Nucl. Phys.* A148: 362 (1970)
52. Kotlinski, B., Bäcklin, A., Clark, D., Cline, D. *Bull. Am. Phys. Soc.* 29: 660 (1984)
53. Vermeer, W. J., Esat, M. T., Fewell, M. P., Spear, R. H., Baxter, A. M., Burnett, S. M. *Phys. Lett.* 138: 365 (1984)
54. Green, S. *Phys. Rev. A* 4: 251 (1972)
55. Arima, A., Iachello, F. *Ann. Rev. Nucl. Sci.* 31: 75–105 (1981)

56. Varnestig, B., Bäcklin, A., Cline, D., Deleplanque, M. A. D., Diamond, R. M., et al. See Ref. 42
57. Emling, E., Fuchs, P., Grosse, E., Kulessa, R., Schwalm, D., et al. *Scientific Rep. 1980, GSI-81-2*, p. 44. Darmstadt: GSI (1981)
58. Guidry, M. W., Lee, I. Y., Johnson, N. R., Butler, P. A., Cline, D., et al. *Phys. Rev.* C20: 1814 (1979)
59. Sayer, R. O., Eichler, E., Johnson, N. R., Hensley, D. C., Riedinger, L. L. *Phys. Rev.* C9: 1103 (1974)
60. Lee, I. Y., Cline, D., Simon, R. S., Butler, P. A., Colombani, P., et al. *Phys. Rev. Lett.* 37: 420 (1976)
61. Kotlinski, B., Bäcklin, A., Cline, D., Wu, C. Y., Diamond, R. M., et al. See Refs. 18, 41
62. Cline, D. *Bull. Am. Phys. Soc.* 21: 962 (1978)
63. Bohn, H., Faestermann, T., Feilitzsch, F. V., Kienle, P., Emling, H., et al. *Scientific Rep. 1981, G.S.I.-82-1*, p. 50. Darmstadt: GSI (1982)
64. Lauterbach, Ch., de Boer, J., Mittag, Ch., Riess, F., Schandera, Ch., et al. *Phys. Lett.* 140B: 187 (1984)
65. Ower, H., Elze, Th. W., Idzko, J., Stelzer, K., Grosse, E., et al. *Nucl. Phys.* A388: 421 (1982)
66. DeVito, R. P., Emling, H., Kulessa, R., Simon, R. S., Briancon, Ch., Lefebvre, A., Evers, D. *Ann. Rep. 1980*, p. 47. Darmstadt: GSI (1981)
67. Grosse, E., Balanda, A., Emling, H., Folkmann, F., Fuchs, P., et al. *Phys. Scripta* 24: 337 (1981)
68. Spreng, W., Azgui, F., Emling, H., Grosse, E., Kulessa, R., et al. *Phys. Rev. Lett.* 51: 1522 (1983)
69. Piercey, R. B., Hamilton, J. H., Ramayya, A. V., Emling, H., Fuchs, P., et al. *Phys. Rev. Lett.* 46: 415 (1981)
70. Czosnyka, T., Cline, D., Hasselgren, L., Wu, C. Y., Diamond, R. M., et al. *Nucl. Phys.* A458: 123 (1986)
71. Johnson, A., Ryde, H., Sztarkier, J. *Phys. Lett.* 34B: 605 (1971)
72. Stephens, F. S., Simon, R. S. *Nucl. Phys.* A183: 257 (1972)
73. Schwalm, D., *Nucl. Sci. Conf. Res. Ser., Conf. of High Ang. Mom. Prop. of Nuclei*, ed. N. R. Johnson, 4: 91–118. Harwood Acad. (1983)
74. Andrews, H. R., Häusser, O., Ward, D., Taras, P., Rud, N., et al. *Phys. Rev. Lett.* 45: 1835 (1980)
75. Häusser, O., Gräf, H., Grodzins, L., Jaeschke, E., Metag, V., et al. *Phys. Rev. Lett.* 48: 383 (1982)
76. Seiler-Clark, G., Pelte, D., Emling, H., Balanda, A., Grein, H., et al. *Nucl. Phys.* A399: 211–29 (1983)
77. Kulessa, R., De Vito, R. P., Emling, H., Grosse, E., Schwalm, D., et al. *Z. Phys.* A312: 135 (1983)
78. Elze, Th. W., Gerl, J., Happ, Th., Keppler, K., Ower, H., *Scientific Rep. 1982 GSI-83-1*, p. 54. Darmstadt: GSI (1983)
79. Davidson, W. F., Warner, D. D., Casten, R. F., Schreckenbach, K., Böner, H. G., et al. *J. Phys.* G-7: 455 (1981)
80. Gerl, J., Elze, Th. W., Ower, H., Ronge, K., Bohn, H., Faestermann, T. *Phys. Lett.* 120B: 83 (1983)
81. Gerl, J., Elze, Th. W., Ower, H., Bohn, H., Faestermann, T., et al. *Phys. Rev.* C29: 1684 (1984)
82. Bohr, A., Mottelson, B. R. *Nuclear Structure*, Vol. 2. Reading: Benjamin (1975)
83. Russo, P., Sprinkle, J. K., Cline, D., Vold, P. B., Scharenberg, R. P. *Univ. Rochester Nucl. Struct. Res. Lab. Ann. Rep.*, p. 79 (1978)
84. Glenn, J. E., Pryor, R. J., Saladin, J. X. *Phys. Rev.* 188: 1905 (1969)
85. Davydov, A. S., Filippov, G. F. *Nucl. Phys.* 8: 237 (1958)
86. Bolotin, H. H., Stuchberry, A. E., Morrison, I., Kennedy, D. L., Ryan, C. G., Sie, S. H. *Nucl. Phys.* A370: 146 (1981)
87. Mauthofer, A., Ower, H., Stelzer, K., Elze, Th. W., Idzko, J. See Ref. 23, p. 64
88. Günther, C., Hübel, H., Kleinrahm, A., Kulessa, R., Emling, H., et al. *Z. Phys.* A301: 119 (1981)
89. Kishimoto, T., Tamura, T. *Nucl. Phys.* A270: 317 (1976)
90. Fahlander, C., Bäcklin, A., Hasselgren, L., Kavka, A., Mittal, V., et al. *Precommunications to the Niels Bohr Centenn. Symp. on Nucl. Struct.*, p. 45. Copenhagen: Niels Bohr Inst. (1985)
91. Stachel, J., Hill, P., Kafrell, N., Emling, H., Grien, H., et al. *Nucl. Phys.* A419: 589–620 (1984)
92. Srebrny, J., Cline, D., Wu, C. Y., Diamond, R. M., Habs, D., et al. *Proc. Int. Conf. on Extreme States in Nuclear Systems, Rossendorf*, ed R. Arlt, B. Kuhn, p. 72. Dresden: Zentralinst. Kernforsch (1980)
93. Brussermann, S., Lieb, K. P., Sona, P., Emling, H., Gross, E., et al. *Scientific Report 1984, GSI-85-1*, p. 74. Darmstadt: GSI (1985)
94. Winther, A., Alder, K. *Nucl. Phys.* A319: 518 (1979)

Annual Review of Nuclear and Particle Science
Volume 36, 1986

CONTENTS